Crystal structure of ED-Eya2: insight into dual roles as a protein tyrosine phosphatase and a transcription factor

Suk-Kyeong Jung,* Dae Gwin Jeong,* Sang J. Chung,† Jae Hoon Kim,‡,§ Byoung Chul Park,* Nicholas K. Tonks,‖ Seong Eon Ryu,‡,#,1 and Seung Jun Kim*,‖,1

*Medical Proteomics Research Center, †BioNanotechnology Research Center, and ‡Systemic Proteomics Research Center, Korea Research Institute of Bioscience and Biotechnology, Daejeon, Korea; §Faculty of Biotechnology, College of Applied Life Science, Cheju National University, Jeju, Korea; ‖Cold Spring Harbor Laboratory, Cold Spring Harbor, New York, New York, USA; and #Department of Bioengineering, Hanyang University, Seoul, Korea

ABSTRACT **Eya proteins are transcription factors that play pivotal roles in organ formation during development by mediating interactions between Sine Oculis (SO) and Dachshund (DAC). Remarkably, the transcriptional activity of Eya proteins is regulated by a dephosphorylating activity within its Eya domain (ED). However, the molecular basis for the link between catalytic and transcriptional activities remains unclear. Here we report the first description of the crystal structure of the ED of human Eya2 (ED-Eya2), determined at 2.4-Å resolution. In stark contrast to other members of the haloacid dehalogenase (HAD) family to which ED-Eya2 belongs, the helix-bundle motif (HBM) is elongated along the back of the catalytic site. This not only results in a structure that accommodates large protein substrates but also positions the catalytic and the SO-interacting sites on opposite faces, which suggests that SO binding is not directly affected by catalytic function. Based on the observation that the DAC-binding site is located between the catalytic core and SO binding sites within ED-Eya2, we propose that catalytic activity can be translated to SO binding through DAC, which acts as a transcriptional switch. We also captured at two stages of reaction cycles-acyl-phosphate intermediate and transition state of hydrolysis step, which provided a detailed view of reaction mechanism. The ED-Eya2 structure defined here serves as a model for other members of the Eya family and provides a framework for understanding the role of Eya phosphatase mutations in disease.—Jung, S.–K., Jeong, D. G., Chung, S. J., Kim, J. H., Park, B. C., Tonks, N. K., Ryu, S. E., Kim, S. J.. Crystal structure of ED-Eya2: insight into dual roles as a protein tyrosine phosphatase and a transcription factor. *FASEB J.* 24, 560–569 (2010). www.fasebj.org**

Key Words: branchio-oto-renal syndrome · eyes absent phosphatase · halo-acid dehalogenase

THE COORDINATED ACTIONS OF protein tyrosine phosphatases (PTPs) and protein tyrosine kinases control essential cellular signaling involved in regulating cell growth, differentiation, transcription, and metabolism (1). The human PTP family, which consists of 107 members, comprises three classes of Cys-based PTPs and one class of Asp-based PTPs, defined by their substrate specificity and structural characteristics (2). Although Cys-based PTPs have been well characterized biologically and structurally, Asp-based Eya phosphatases have only recently been characterized as PTPs. Eya phosphatases do not resemble Cys-based PTPs, which use cysteine as a nucleophile in a catalytic reaction that involves a thiol-phosphate intermediate. Instead, Eya phosphatases use aspartic acid as a nucleophile in a metal-dependent reaction.

Four isoforms of Asp-based Eya phosphatases are conserved among different species of mammals and other organisms, including plants. Eya phosphatases have a C-terminal Eya domain (ED) of ~275 aa in common and have some homology to the haloacid dehydrogenases (HADs) (3, 4). Most Eya phosphatases have a transcription-activating domain at the N terminus that comprises ~200–250 aa. *Eya* genes were identified initially for the critical role they played in diverse developmental processes in metazoans. For example, hypomorphic *eya* alleles in *Drosophila* result in loss or severe defects of the eye. Complete knockout of *eya* function is embryonically lethal, the result of defects in head morphology, gonad formation, and body wall musculature (5). In the *Drosophila* eye, the ED of Eya phosphatases has been shown to bind two retinal determination proteins, Sine Oculis (SO) and Dachshund (DAC), which mediate transcriptional activation of downstream genes (6, 7). The recent identification of the ED as a PTP ascribed a second essential function to Eya (8–11). That Eya's transcriptional role might somehow depend on its PTP activity has been suggested by recent studies, which have shown that disruption of

[1] Correspondence: S.J.K., Medical Proteomics Research Center, Korea Research Institute of Bioscience and Biotechnology, 52 Eoeun-Dong, Yuseong-Gu, Daejeon, 305-600, Korea. E-mail: ksj@kribb.re.kr; S.E.R., Department of Bio Engineering, Hanyang University, Seongdong-Gu, Seoul 133-791, Korea. E-mail: ryuse@hanyang.ac.kr

doi: 10.1096/fj.09-143891

0892-6638/10/0024-0560 © FASEB

PTP activity correlates strongly with its transcriptional activity and related role in organ formation (8–10). Quite recently, Eya phosphatases are known to be involved in DNA damage repair by regulating the level of phosphorylation at the C-terminal tyrosine residue of H2A.X (12, 13).

Although the function and regulation of Eya phosphatases have been studied extensively, their molecular architecture is largely unknown. Eya phosphatases belong to the HAD structural family, but sequence homology between the ED of Eya and HAD members is very low and limited to 3 conserved catalytic motifs. Further, the ~130 residues of the inserted helix-bundle motif (HBM) in the ED are not similar to any HAD members (14). An understanding of Eya phosphatase catalysis mechanisms, substrate specificity, and interactions with DAC and SO requires structural investigation. We showed previously that ED-Eya had an unusually negative charged surface that helps accommodate histone H2A.X as a substrate (13). Here we report the crystal structure of human ED-Eya2 at 2.4-Å resolution in detail. Its helices are unexpectedly elongated along the back of the active site, in contrast to the helices of known HADs, which are tightly packed and capped over the active site. This unusual association provides insight into how its two functions—phosphatase and transcription factor—can be regulated. Together with a native structure, we report here two complexed structures mimicking phosphoenzyme intermediate and transition state analog bound. These provide new insight into the reaction mechanism for substrate binding and for phosphotransfer reaction. Our analysis of ED-Eya2 establishes a structural basis for substrate specificity and a framework for understanding mutations that lead to defective Eya phosphatases associated with human branchio-oto-renal (BOR) syndrome, deafness, and optical defects (ODs) (15, 16).

MATERIALS AND METHODS

Expression and purification

A full-length clone of human Eya2 (gene accession no. BC008803; OpenBiosystems, Huntsville, AL, USA) was subcloned into pET28a. ED-Eya2 (residues 268–538) was expressed in the BL21 (DE3) strain of *Escherichia coli*. Cells were grown at 295 K after induction with 0.1 mM IPTG for 20 h. Cells were harvested and suspended in buffer containing 50 mM Tris-HCl (pH 7.5), 500 mM NaCl, 1 mM PMSF, 0.05% (v/v) 2-mercaptoethanol, and 5% (v/v) glycerol. After lysing cells by sonication, His-tagged ED-Eya2 was purified using nickel-affinity chromatography, and the histidine-tag was removed by thrombin protease digestion. ED-Eya2 was purified further by DEAE-Sepharose FF ion exchange chromatography and gel filtration chromatography, then equilibrated with buffer containing 20 mM HEPES–NaOH (pH 7.0), 0.2 M NaCl, 5 mM $MgCl_2$, 2 mM DTT, and 5% glycerol. The catalytic activity of ED-Eya2 was determined using a spectrofluorometric assay (see Supplemental Data). To prevent protein oxidation, 20 mM DTT was added, and the protein was concentrated to 18 mg/ml for crystallization.

Crystallization and data collection

Crystallization was performed at 291 K using the hanging-drop vapor diffusion method. Initial trials were performed using commercial screening kits (Hampton Research, Aliso Viejo, CA, USA). Optimal crystals were formed by mixing 1.8 μl of protein solution with an equal volume of reservoir solution containing 0.1 M bis-Tris (pH 6.0) and 2.4 M NaCl and growing for 3 d. X-ray diffraction data were collected on the Pohang Accelerator Laboratory (Pohang, Korea) beamline 4A equipped with an ADSC quantum detector (Area Detector Systems Corp., Poway, CA, USA). For cryoprotection, the crystals were soaked in a reservoir solution containing 20% (v/v) glycerol. The crystal diffracted to 2.4 Å resolution and belonged to the space group *I*4, with unit cell parameters of $a = b = 183.61$ Å, $c = 120.15$ Å, $\alpha = \beta = \gamma = 90°$. The collected diffraction data were processed and scaled with Mosflm (17) and Scala (18). ED-Eya2 complexed with AlF_3 (or with BeF_3) was obtained by reacting purified ED-Eya2 with 0.1 mM of $AlCl_3$ (or 0.1 mM $BeCl_3$) and 10 mM of NaF for 30 min at 277 K. The complexed crystals were grown under the same conditions as native crystals. X-ray diffraction data were collected at SPring8 (Hyogo, Japan) beamline BL38B1. The collected diffraction data were processed and scaled using Denzo and Scalepack software (19). Data collection statistics are shown in **Table 1**.

Structure solution and refinement

The structure of ED-Eya2 was determined by the multiple isomorphous replacement method using two heavy-atom derivatives. The first derivative was obtained by soaking native crystals for 1 h in the mother liquor containing 1 mM $KAu(CN)_2$. The second heavy-atom derivative was obtained by soaking for 2 h in mother liquor containing 1 mM $Sm(OAc)_3$. The locations of heavy atoms, heavy-atom parameter refinement, and phase calculation were carried out using the program SOLVE (20). Subsequent solvent flattening and noncrystallographic symmetry (NCS) averaging were performed using the program RESOLVE (20). The resulting electron-density map enabled the building of a majority of the residues. The ED-Eya2 crystal contained four protomers. The initial and iterative model building were performed using the program O (21). However, the crystals tended to show merohedral twinning. To detect merohedral twinning and estimate the twinned fraction, a merohedral crystal twinning server (22) was used. The value of the twinned fraction was 0.35, indicating that the ED-Eya2 crystal was partially twinned, with a twin operator of *h, -k, -l*. The model was refined using the program CNS, taking partial twinning into account (23). NCS restraints were applied during refinement and released in the final stage. The final R_{cryst} and R_{free} were 16.8 and 21.4%, respectively (Table 1). A Ramachandran plot drawn using Procheck (24) showed that 89.5 and 10.2% of all residues lay in the most favored and additionally favored regions, respectively. No residues were found in the disallowed regions. The final model includes the residues 268–355 and 372–538 for protomer A (a model discussed in the text), the residues 268–356 and 375–538 for protomer B, the residues 268–355 and 372–538 for protomer C, the residues 268–356 and 372–538 for protomer D, 4 magnesium ions, and 115 water molecules. For protomers A and C, the 3 residues preceding the N terminus of the thrombin cleavage site were included in the model. The native ED-Eya2 model was taken as a starting point for refinement of complexed ED-Eya2, and the same refinement protocols of native ED-Eya2 were applied. Although electron densities for AlF_3 or BeF_3 were evident, these were built into the structure at the final stage of the refine-

TABLE 1. *Data collection, phasing, and refinement statistics*

Statistic	Native	Gold[a]	Samarium[b]	BeF_3	AlF_3
Resolution limit (Å)	2.4	2.5	2.7	2.5	2.5
Observations	360,049	336,289	256,298	504,660	484,549
Unique reflections	77,791	68,979	50,520	68,947	68,352
Completeness (%)[c]	99.8 (99.9)	99.9 (99.9)	94.1 (95.2)	99.7 (98.4)	99.8 (99.9)
Multiplicity	4.6 (4.7)	4.9 (5.0)	5.1 (5.1)	7.3 (6.5)	7.1 (6.4)
$I/\sigma I$	6.9 (2.5)	7.1 (3.8)	7.0 (2.3)	26.9 (2.4)	25.7 (2.4)
R_{merge} (%)[d]	7.9 (29.3)	7.0 (19.8)	7.7 (33.0)	7.4 (44.4)	8.4 (55.1)
Heavy-atom sites		6	3		
Refinement					
Resolution range (Å)	50–2.4			50–2.5	50–2.5
Reflections[e]	76,896 (3694)			64,507 (3281)	62,438 (3066)
Atoms (protein/nonprotein)	8268/119			8292/159	8274/163
R_{cryst}/R_{free} (%)	16.8/21.4			22.4/25.4	20.0/24.0
RMS deviation					
Bond distances (Å)	0.008			0.007	0.008
Bond angles (deg)	1.27			1.25	1.30
Impropers (deg)	0.74			0.73	0.70
Dihedral angles (deg)	21.3			21.4	21.0
Thermal factor ($Å^2$)					
Main-chain atoms	41.3			47.2	44.8
Side-chain atoms	42.1			48.6	46.3
Nonprotein atoms	31.0			36.8	32.7

[a] Potassium gold cyanide. [b] Samarium acetate. [c] Values in parentheses are for the highest-resolution shell. [d] $R_{merge} = \sum_i I_i - <I>/\sum <I>$, where I is the intensity for the ith measurement of an equivalent reflection with the indices h, k, l. [e] Values in parentheses are for the R_{free} data set.

ment. Figures were drawn using the programs Ribbons (25), Molscript (26), and PyMol (Molecular Graphics System; http://www.pymol.org).

RESULTS

Overall structure

We determined the structure of ED-Eya2 using the multiple isomorphous replacement method at 2.4-Å resolution. Because other Eya members have ~60% sequence identity with Eya2, they are likely to be folded similarly. The 4 protomers (A–D) in the asymmetric unit had similar conformations and formed 2 potential dimers (A:B and C:D) related by 2-fold NCS. However, a gel-filtration experiment indicated that ED-Eya2 exists as a protomer in solution (data not shown), so these dimeric contacts are not likely to be significant.

The crystal structure (**Fig. 1*A***) shows a novel arrangement comprising 2 domains: a HAD-like catalytic domain consisting of N-terminal (267–282) and C-terminal residues (424–538), and an HBM comprising 7 helices (residues 283–423) that lies between the N- and C-terminal regions. Based on a structural homology search using the DALI server (27), the HAD-like domain was found to possess a typical α/β hydrolase fold and belonged to the HAD family. Several HAD members, including enolase-phosphatase e1 (MASA; PDB code 1yns, Z score=12.3) (28), sugar phosphate phosphatase bt4131 (PDB code 1ymq, Z score=11.4) (29), L-2 haloacid dehalogenase (PDB code 1qq5, Z score=10.6) (30), and phosphoserine phosphatase (PSP; PDB code 1f5s, Z score=9.7) (31) were identified. An alignment of ED-Eya2 with MASA superposed 104 of 140 Cα atoms with a root mean square (RMS) deviation of 1.5 Å (Fig. 1*B*). The HAD-like domain contains a parallel, 5-stranded β sheet (β1–β5) flanked by 4 helices (α8, α10–α12). Helix α9 is inserted between strands β2 and β3 and is positioned in the direction of the β sheet. A structural homology search using DALI (27) showed that, in contrast to the HAD-like domain, the HBM of Eya2 has no structural homologue with a Z score > 4.0. The HBM is composed solely of 7 helices that are elongated across the back side of the catalytic domain and wrap around helix α9 of the catalytic domain.

Active site

The active site shared by members of the HAD family is defined by 3 conserved sequence motifs (Figs. 1*B* and **2*A***) and a bound magnesium ion. The conserved residues, which are critical in catalysis, are generally well aligned, which suggests that Eya shares a common catalytic mechanism with other HADs. Based on the structural alignment with MASA, Asp274 is well superposed with a nucleophile in MASA. Asp274 is positioned optimally and anchored by a magnesium ion. Asp276 is predicted to act as a general acid/base by stabilizing the leaving group during the first step and is then involved in activating water-mediated hydrolysis of the phosphoenzyme complex. Asp276 is directed toward the active site and occupies a position similar to that of general acid/base residue in MASA. Thr278 is positioned in the β-turn structure and contacts Asp274 and Asp502. This

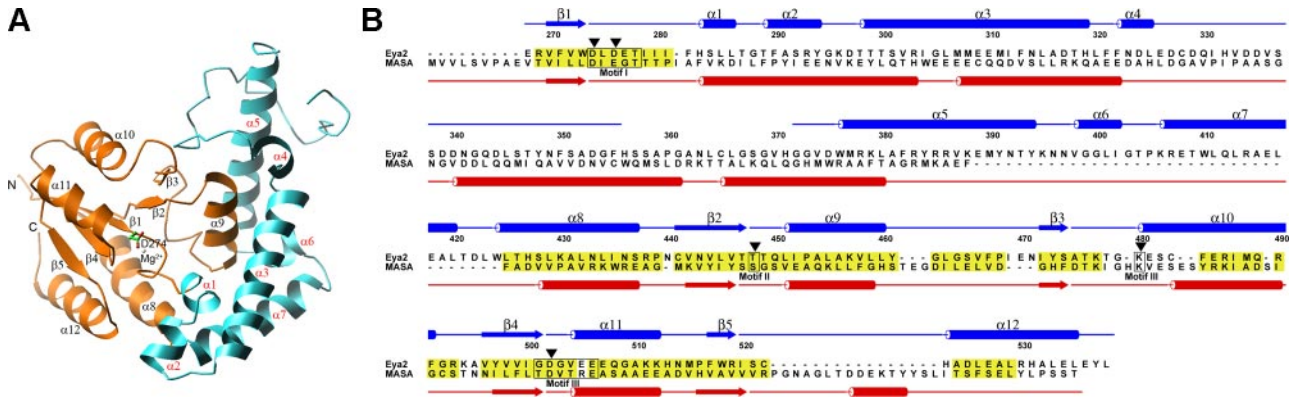

Figure 1. ED-Eya2 structure. *A*) Ribbon diagram of ED-Eya2. Catalytic domain (orange) and HBM (cyan). The catalytically active Asp274 and magnesium ion are drawn as ball-and-stick models. Secondary structural elements defined by the program Procheck (21) are labeled on the drawing. Secondary structural elements (and boundaries) are β1 (270–274), β2 (441–447), β3 (472–474), β4 (496–501), β5 (517–519), α1 (283–286), α2 (289–294), α3 (298–319), α4 (322–325), α5 (376–394), α6 (398–401), α7 (406–420), α8 (424–437), α9 (451–460), α10 (480–491), α11 (504–512), and α12 (523–535). *B*) Structure-based alignment of Eya2 with MASA. Superposition was performed using the O program (18) using the criteria of <3.8 Å for >3 consecutive Cα atoms. In the resulting alignment, 104 Cα atoms were superposed, with an overall RMS deviation of 1.5 Å. Superposed residues are shaded yellow. Eya2 secondary structural elements (blue) appear above the alignment; those of MASA (red) are below the alignment. Catalytically important residues are indicated by inverted arrowheads. Residues corresponding to consensus motifs of HAD family are enclosed in the box.

interaction may help two aspartates coordinate a magnesium ion and may be crucial for enzymatic function. Lys480 is predicted to play a role in substrate binding. Although the Cα position of Lys480 in Eya2 is different from that of the equivalent residue in MASA (28), the side chain occupies a similar position. In motif III, the side chain of another glutamate (Glu506), strictly conserved in Eya homologs, is positioned at the rim of the active site and contributes a negative charge to the active-site cradle. These structural observations are consistent with the observation that the corresponding mutations result in a marked decrease in *in vitro* phosphatase activity (8–10, 32).

Structure of BeF3-Eya2 complex mimicking a phosphoenzyme intermediate

Complexation with BeF_3 did not lead to drastic alteration in overall structure, but some significant differences were found (Supplemental Fig. S1*A*, *B*). The superposition of BeF3-complexed ED-Eya2 structure with that of the native structure shows that the α4-α5 loop, β2-α9 loop, and β3-α10 loop move toward BeF_3 molecule. These loops are spatially concentrated on one region that includes catalytic motif II (Supplemental Fig. S1*B*), which suggests that this region has an intrinsic mobility that allows lateral movement on substrate binding.

The beryllium atom of BeF_3 is covalently attached to OD1 atom of Asp274 with nearly ideal tetrahedral geometry, mimicking a stable phosphor-aspartyl enzyme intermediate (Fig. 2*B*). The 3 fluorine ions of BeF_3 engage in extensive interactions with side-chain atoms of Thr447, Thr448, Lys480, a main-chain atom of Asp276, and a magnesium ion, which might stabilize the complex in the intermediate state. Another notable change is that the side chain of Asp276 moves ~2.4 Å toward the BeF_3 molecule, confirming the role of Asp276 as a general acid/base in the Eya phosphatase. The shift of Asp276 is coupled to creation of an ordered water molecule between Asp276 and Glu277 (OD1 in Asp276–OH_2 in Wat1, 2.7 Å; OE1 in Glu277–OH_2 in Wat1, 2.6 Å; Fig. 2*B*). This geometry would be expected to facilitate formation and cleavage of the P-O bond between Asp274 and the phosphate group by activating a water molecule (Fig. 2*C*). In protein tyrosine phosphatase 1B (PTP1B), a prototype of Cys-based PTPs, a general acid/base (Asp181) is not sufficient for complete catalysis; a glutamine residue (Gln262) near Asp181 is thought to help facilitate the second step of the catalytic reaction by activating a water molecule. A mutation at this glutamine resulted in a 100-fold decrease in catalytic activity, suggesting that it is critical for hydrolysis of the phosphoenzyme complex (33). Glu277 in Eya2 might also indirectly assist a water molecule for attack during the hydrolysis of the phosphoenzyme complex.

Structure of AlF3-Eya2 complex mimicking a transition state of phosphoenzyme

AlF_3 occupies a nearly identical position to that of BeF_3 in ED-Eya2-BeF_3 complex, but AlF_3 adopts a planar instead of tetrahedral geometry (Fig. 2*D*). The aluminum atom is 2.0 Å from the OD1 atom of Asp274, and 3 fluorine ions have similar interactions with those of the BeF_3-complexed structure. One notable exception is that a water molecule optimal for nucleophilic attack is not seen in AlF_3-complexed ED-Eya2. In the case of both phosphoserine phosphatase (34) and Fcp1 complexed with aluminum fluoride (35), a water molecule sits above the aluminum fluoride plane, maintaining a

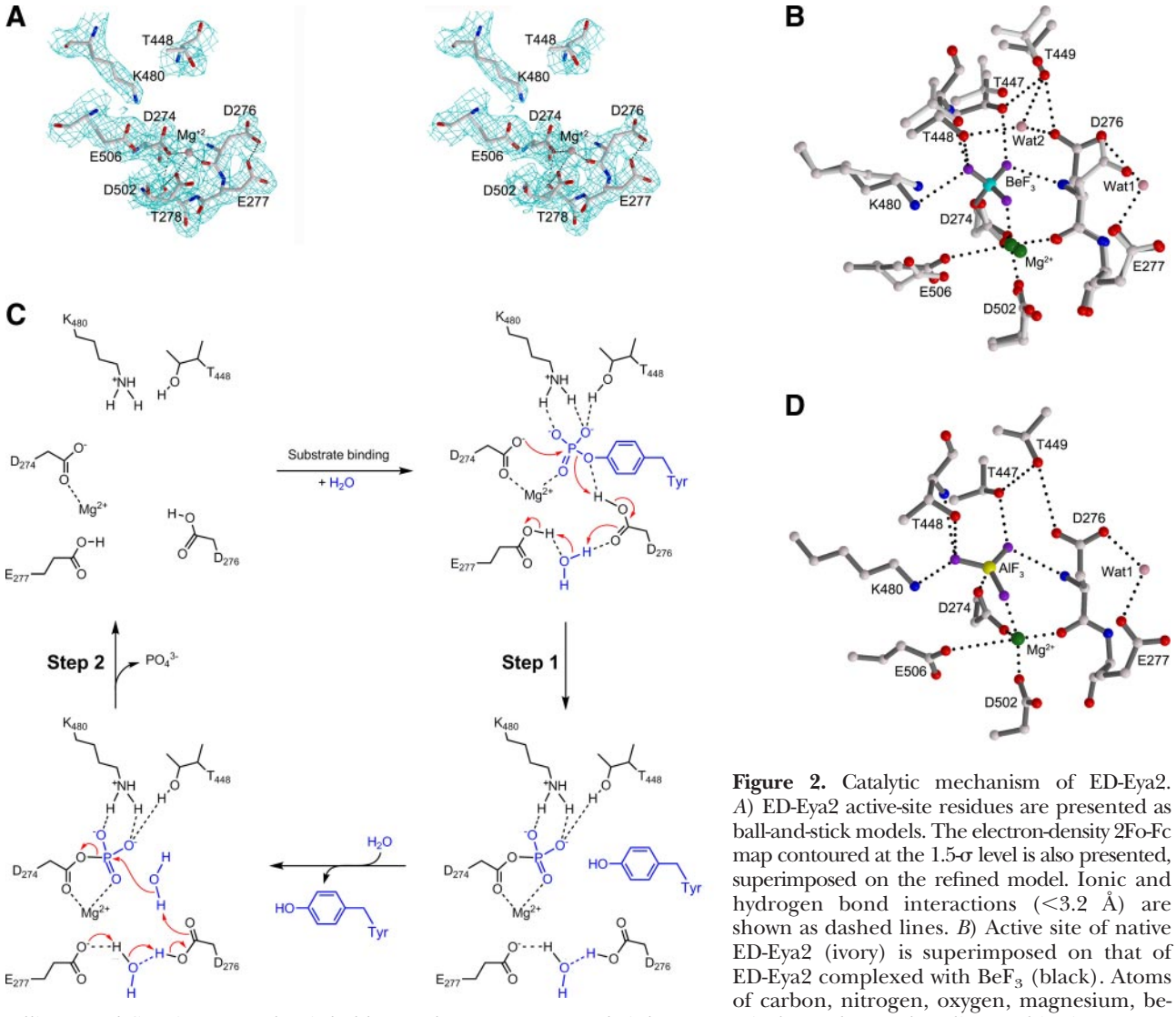

Figure 2. Catalytic mechanism of ED-Eya2. *A*) ED-Eya2 active-site residues are presented as ball-and-stick models. The electron-density 2Fo-Fc map contoured at the 1.5-σ level is also presented, superimposed on the refined model. Ionic and hydrogen bond interactions (<3.2 Å) are shown as dashed lines. *B*) Active site of native ED-Eya2 (ivory) is superimposed on that of ED-Eya2 complexed with BeF_3 (black). Atoms of carbon, nitrogen, oxygen, magnesium, beryllium, and fluorine are pale pink, blue, red, green, cyan, and violet, respectively. Hydrogen bonding and ionic contacts around the active site of complexed ED-Eya2 are represented by dashed lines. *C*) A hypothetical 2-step reaction mechanism for ED-Eya2. A water molecule between Asp276 and Glu277 facilitates the formation and the breakdown of the phosphoenzyme complex by assisting the general acid/base, Asp276. *D*) Active site of ED-Eya2 complexed with AlF_3.

good geometry for nucleophilic attack—an architecture supportive of an associative reaction pathway. In AlF_3-complexed ED-Eya2, the nearest water molecule is distant from the aluminum atom (~3.6 Å) and does not have inline geometry with respect to the Al-O bond for nucleophilic attack (water, aluminum, and OD1 of Asp274 subtend a 138° angle). Further, this water is not coordinated with a general base, Asp276. This finding suggests little participation of solvent molecule as a nucleophile during C-O bond breakage. Thus, we propose that ED-Eya2 catalyzes hydrolysis *via* a dissociative mechanism, instead of addition-elimination pathway. However, we do not preclude the possibility of associative reaction pathway at this medium resolution.

Structure of HBM in ED-Eya2 is distinct

Whereas the HAD catalytic domains are structurally well conserved, the intervening HBMs are structurally divergent, perhaps conferring specificity and variety to members of the HAD family (14). Despite their structural diversity, the HBMs of different HAD members share certain features. HBMs are usually composed of 4 helices and are located at the top of the active site, thus constituting a potential pocket for specific substrates. Although the orientation and location of HBMs differ, HBMs cover the active site and thus restrict substrate access (**Fig. 3**). Access to the active-site pocket varies according to the individual enzyme and its specific substrate. However, the HBM in Eya2 is completely distinct in several aspects. First, it consists of 140 aa (other HADs have 55–105) (14) and has 7 helices in an elongated arrangement (other HADs have 4 tightly packed helices). A homology search using the DALI server (27) also confirmed that the folding of HBM in ED-Eya2 is unique (similarity <4 in terms of *Z* score). However, the most prominent difference is the mode of association with the catalytic domain. In ED-Eya2, the 7

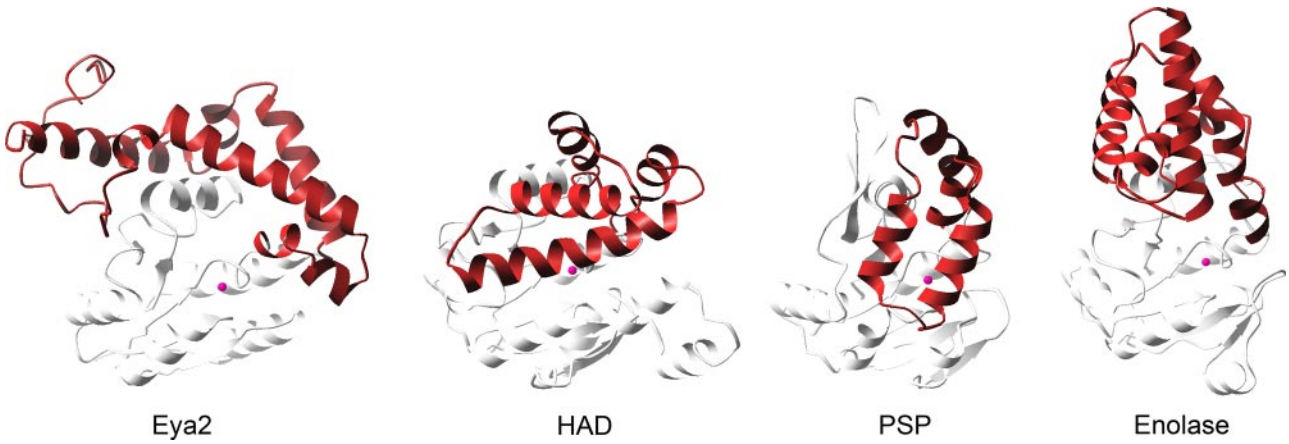

Figure 3. Structural comparison between Eya2 and other HAD proteins. Schematic diagrams showing the Eya2, haloacid dehalogenase (PDB code 1QQ5), phosphoserine phosphatase (PDB code 1L7P), and enolate phosphatase E1 (PDB code 1YNS), drawn to a common orientation and scale. Catalytic domain and HBM are colored differently, and the position of the active site magnesium ion is shown as a purple sphere to represent the location of the catalytic core.

helices traverse the outside of the catalytic domain and result in a completely open active site (Fig. 3). The open active site might help protein substrates, including H2A.X, access the site and facilitate catalysis (13).

Role of mutations in Eya-related disorders

The high level of similarity among the primary sequences of Eya phosphatases suggests that the structures of Eya family members may also be similar. Using the ED-Eya2 structure as a platform, we examined disease-associated Eya mutations to investigate possible relationships between mutation positions and pathogenic effects. To date, >100 Eya mutations have been reported (3, 4). Most are nonsense, insertion/deletion, or splice-site mutations. Fifteen missense mutations that often lead to BOR syndrome, deafness, OD, and loss of function in *Drosophila* alleles (36–39) can be used to identify residues that are important for protein function or stability (**Table 2** and **Fig. 4*A***). To gain further insight into the roles of each mutation, we also calculated fractional solvent accessibility (FSA) for the side chain of each residue and the change in protein stability induced by mutations (40). These are excellent tools for investigating potential protein–protein interactions and protein structure-destabilizing mutations. Overall, mutations of residues that have low FSA values are predicted to have a substantial negative effect on protein stability.

The studied mutations can be grouped into catalytic active site, protein core, and protein surface mutations according to the positions of the native residues. At 6 sites within the hydrophobic core of the protein, mutation results in the replacement of the original residue with a bulkier or altered charged residue: V270E, Q330X, T421I, N433P, L451R, and L529P (where X

TABLE 2. *Mutations in the ED of Eya phosphatases*

Corresponding residue in Eya2	Mutation	Protein studied	Related diseases or loss of function	Roles in Eya2 structure[a]	Predicted ΔΔG upon mutation[b]
Val270	V→E	hEya1	BOR	Str./0.03	>10
Thr278	T→M	hEya1/mEya3/Fly	Eya loss of function	Str., Cat./0.0	6.20
Met307	R→X[5]	hEya1	BOR	−/0.49	−
Glu309	E→K	hEya1/mEya3/Fly	OD	−/0.37	2.00
Gln330	Q→X	hEya1	BOR	Str./0.04	−
Gly372	G→S	hEya1/mEya3/Fly	BOR/OD	−/0.96	3.64
Asp375	D→G	hEya1	BOR/Deafness	−/0.75	3.94
Arg386	R→Q	hEya1	BOR/Deafness	−/0.26	0.89
Gly400	G→R	hEya1	BOR	−/0.47	−1.87
Thr421	T→I	hEya1/mEya3/Fly	Eya loss of function	Str./0.02	1.78
Asn433	S/L→P	hEya1/mEya3/Fly	BOR	Str./0.01	>10
Leu451	L→R	hEya1/mEya3/Fly	BOR	Str./0.02	>10
Arg493	R/K→G	hEya1/mEya3/Fly	OD	−/0.93	1.15
Gly501	G→E	hEya1/mEya3/Fly	Eya loss of function	Str., Cat./0.0	>10
Leu529	L→P	hEya1/Fly	BOR	Str./0.02	>10

Str., structural role; Cat., catalytic role; X, any amino acid. [a]Values on right are fractional solvent accessibility (FSA) for each residue, calculated using the program QUANTA as the ratio of the side-chain FSA for residue X to the FSA obtained after reducing the structure to a Gly-X-Gly tripeptide. [b]Values of mutation-induced stability change (ΔΔG) relative to wild type.

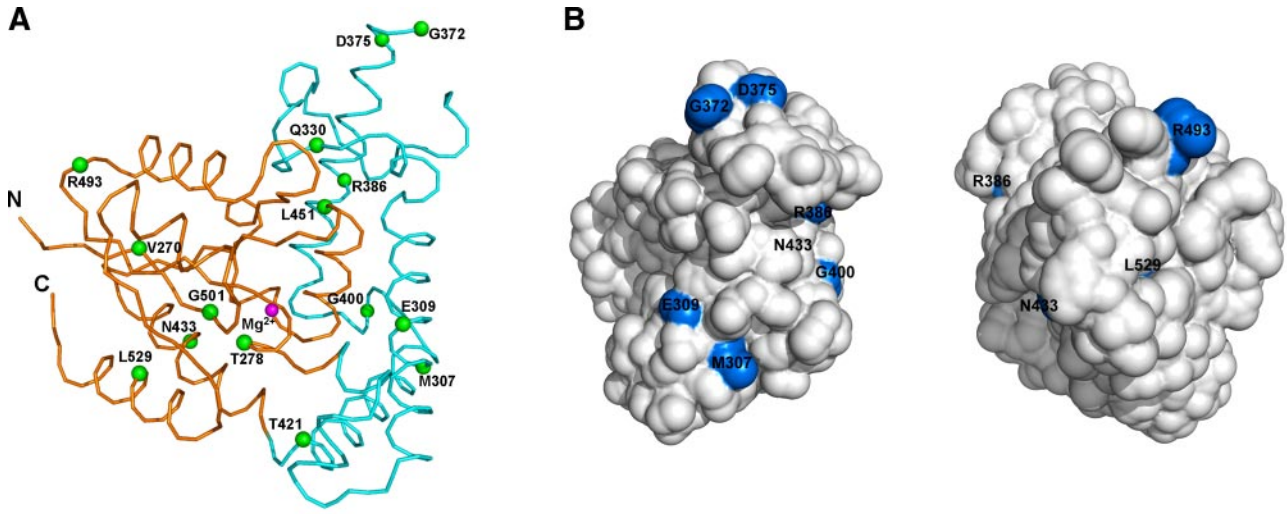

Figure 4. Missense disease mutations. *A*) Cα positions of missense mutations found in Eya homologs are shown as green spheres on a worm model of ED-Eya2. Magnesium ion is represented to indicate catalytic core. Point of view and color-coding scheme are the same as in Fig. 1*A*. *B*) Missense mutations (blue) on the surface of the ED-Eya2 structure, mapped from the Eya homologs in blue. Left: view facing the HBM. Diagram is rotated 90° along the *y* axis from the viewpoint of *A*. Right: opposite view from that of *A*.

indicates any residue); most of these substitutions are predicted to destabilize the protein. One exception is the T421I mutation, which probably does not have a major effect on stability because it does not substantially increase size or alter the charge. Two missense mutations, T278M and G501E, with FSA values approaching zero, occur at residues that have been implicated in catalytic activity. As noted earlier, the side chain of Thr278 forms hydrogen bonds with the crucial Asp274 and Asp502 residues. Gly501 is a strictly conserved residue in motif III. Mutation of these two residues might affect core structure as well as catalytic function. The remaining missense mutations (7 of 15) have FSA values larger than 0.25 and correspond to solvent-exposed residues. The positions of these residues suggest that they may be protein partner binding sites and may thus have the potential to influence transactivation function. Six of seven solvent-exposed mutations are found on the same face of HBM at a distance from the catalytic side. Two pairs of solvent-exposed missense mutations, G372S/D375G and M307X/E309K, are clustered on the same face of HBM opposite the active site (Fig. 4*B*). Two other mutations, R386Q and G400R, are located at isolated positions on the same face. G372S is located in the α4-α5 loop, whereas D375G lies within helix α5; both are situated at the top of the molecule (Fig. 4). Q330X, which is not fully exposed to the solvent, is located within the same region. The second cluster of mutation sites, M307X/E309K, is located on helix α3. The only exception is a mutation of arginine to glycine at residue 493, which is located on the α10-β4 loop on the catalytic face.

Potential binding site for SO is distant from the catalytic site

Mutsuddi *et al.* (36) investigated the relationship between phosphatase and Eya-SO bipartite transcriptional activities using point mutations that cause Eya-related disorders (36). N433P and G501E mutations, located near the catalytic core, and L451R mutation, located at the interface between the catalytic domain and HBM, eliminated phosphatase activity (**Table 3**). Considering that those residues have very low FSA values and are mutated to larger residues, the corresponding muta-

TABLE 3. *Relationship between catalytic and transcriptional activities of mutant Eya*

hEya2	mEya3	PTP activity	Transcription activity	Location in Eya2 structure[2]
N433	$L405P^{BOR}$	−	++	CC
L451	$L423R^{BOR}$	−	+/−	I
R493	$K465G^{OD}$	+	++	C
E309	$E281K^{OD}$	−	−	H
G372	$G344S^{BOR+OD}$	++	−	H
T278	$T250M^{FLY}$	+++	++	CC
T421	$T393I^{FLY}$	−	+	I
G501	$G473E^{FLY}$	−	++	CC

Activity data are from Mutsuddi *et al.* (36). CC, catalytic core; I, interface between domains; C, catalytic domain; H, helix bundle motif.

tions are likely to affect the native structure of the catalytic domain. The R493G mutation, located within the catalytic domain but distant from the catalytic core, resulted in a reduction in phosphatase activity (Fig. 4*A* and Table 3). One exception to the trend toward reduced or absent phosphatase activity was the T278M mutant, which displayed a level of activity similar to that of wild-type Eya. Thr278 is located in the catalytic core, and the hydroxyl group of Thr278 interacts with the crucial Asp274 residue. Because Thr278 is one of three consecutive threonine residues in the primary sequences (Figs. 1*B* and 2*B*), we reasoned that the other two threonine residues might have functionally compensated for the T→M mutation. Interestingly, the corresponding T→A mutation in plant Eya results in approximately a 50-fold reduction in catalytic activity (41). Remarkably, most mutations in the catalytic domain retained significant transcriptional activity, implying that SO-directed transcription is independent of catalytic activity.

In contrast to mutations in the catalytic domain, HBM mutations produced conspicuous effects on transcription. The mutations located at a distance from the catalytic domain (E309K and G372S) resulted in a complete loss of transcriptional activity. Notably, E309K and G372S are exposed to the solvent and have been implicated in BOR/OD diseases. Taken together, these results lead us to propose that a surface of the HBM opposite the catalytic core could be a major interaction site that is required for SO-related transcription, independent of the catalytic domain.

Implications for DAC repression-to-activation switching

DAC/SO-mediated regulation is important for proper transcription and subsequent mammalian organogenesis (9). DAC prevents SO-related transcription by recruiting other corepressors, including NcoR, Sin, and histone deacetylase. In addition, DAC is known to interact strongly with SO and Eya through CREB binding protein (42). However, the phosphatase activity of Eya enables Eya to convert the DAC-SO complex into a transcription activator (9). Using *Drosophila* Eya phosphatase, Bui *et al.* (43) found that SO-binding spanned residues 268–373 while that of DAC spanned residues 371–465 (corresponding to ED-Eya2 residue numbering). Mapping these regions onto the surface of the ED-Eya2 structure reveals that the majority of SO-binding sites lie opposite the catalytic domain, whereas those of DAC lie between the catalytic domain and the SO-binding site (**Fig. 5**). Although the catalytic site overlaps slightly with the potential binding site for SO, Tootle *et al.* (10) showed that mutations at the catalytic site, including Asp274 in Eya2, did not affect the interaction with SO. The observation that the SO-binding site is distant from the catalytic site is consistent with the above analysis and implies that SO binding to Eya may not be related directly to phosphatase function. Thus, bioinformatics tools predict that the surface opposite the catalytic face is as likely a protein interaction surface as the catalytic site (See Supplemental Fig. S2). In contrast, the observation that the DAC-binding site in Eya is in the vicinity of the catalytic core suggests that DAC binding may influence Eya catalytic function.

DISCUSSION

This study represents the first elucidation of structure of ED-Eya2 in a new mechanistic class, aspartate-based PTP. Further, we present the structure of human ED-Eya2 with transition state and intermediate analogues bound that provides insights into the mechanisms by which Eya phosphatase functions. We demonstrate that ED-Eya2 undergoes metal-assisted 2-step reactions *via* phosphoaspartyl intermediate during catalysis. Although additional biochemical evidence is required, we provide the reaction mechanism through which the transition state could proceed *via* dissociation. The structure reveals that ED-Eya2 has the common fold to that of HAD but also has several characteristics that are divergent from those of HADs. The crystal structure was found to have an unusual association between the catalytic domain and the HBM.

Although the interactions of Eya with other proteins

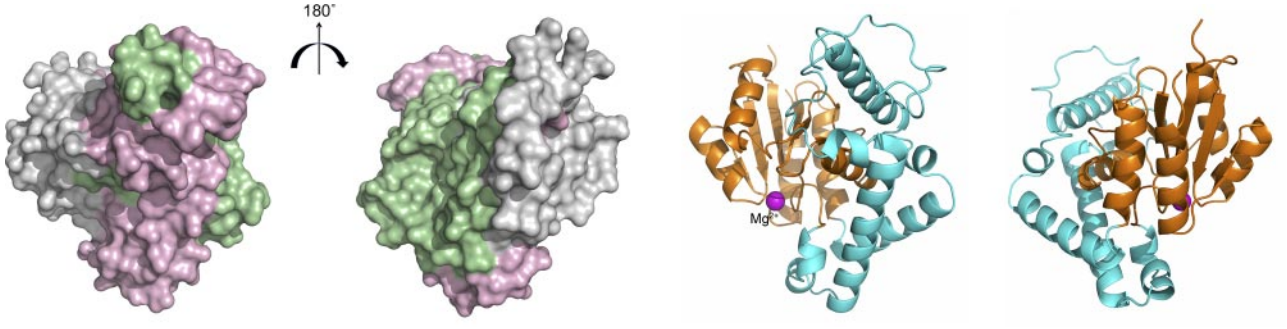

Figure 5. Putative binding sites for SO and DAC. Putative SO- and DAC-binding sites are represented on a surface of the ED-Eya2 structure (left pair). SO-binding surfaces are green; DAC-binding surfaces are magenta. Remaining molecular surfaces are gray. Right image of the pair was produced by rotating the left-hand viewpoint ~180° along the *y* axis. Each ribbon diagram is represented with the same viewpoint in the left pair. Bound magnesium ion is shown as a pink sphere to indicate the location of the catalytic core.

require further investigation, we could propose that transcription factors interact at a surface that is distinct from the catalytic site using structural and biochemical information. Further, using bioinformatics tools, we predicted a location for the potential interacting region, showing that a surface of the HBM opposite catalytic face is a good candidate for protein-protein interactions (Supplemental Fig. S2).

Two conceptually distinct mechanisms may govern the relationship between the dual functions of Eya phosphatase (4, 11). One is that phosphatase and transcription factor activity are tightly linked, functionally and structurally. Alternatively, transcription may operate in a phosphatase-independent manner. Although evidence exists to support each mechanism, our model allows us to speculate on the relationship between catalytic and transcriptional activities in a structural context. As noted earlier, the catalytic site and SO-interacting site are spatially separated. Thus, Eya can fulfill its transcriptional function with SO independent of its phosphatase function. The fact that catalytically impaired Eya mutants and SO retained high basal transcriptional activities supports this notion (10). However, in other contexts, DAC plays a critical role in transcription (9, 11). During transcriptional repression, DAC in a complex with its corepressor prevents SO from binding to the transcription machinery. However, DAC binds to Eya, where it is held between the catalytic domain and SO-binding site within Eya. Eya then dephosphorylates an as-yet-unknown substrate (possibly DAC or a corepressor complex), possibly triggering a conformational transition of the flanking DAC with its corepressor complex. This could concomitantly affect the interface between DAC and SO, allowing the detachment of the corepressor complex from DAC and exposing a new Eya-DAC-SO binding interface that could recruit related transcriptional coactivators. Caught in the middle, DAC appears to act as a transcriptional switch by translating Eya catalytic function into SO-directed transcription. It is also worth noticing that the loop movement in trapped intermediate structure is propagated from active site to DAC binding site (Supplemental Fig. S1*B*). Additional mutational analyses based on the crystal structure presented here and follow-up functional studies will help to clarify further the relationship among Eya, DAC, and SO.

In summary, the catalytic part is spatially separated from the transcriptional part, which enables ED-Eya to act independently as a phosphatase and a transcription factor. Our studies provide a structural basis for understanding the Eya-SO-DAC network in terms of phosphatase function and disease-associated mutations and, by extension, should have implications for mammalian organogenesis. FJ

The authors thank the staff of Pohang Accelerator Laboratory 4A Macromolecular Crystallography Wiggler Beamline (Pohang, Korea) and SPring8 BL38B1 (Hyogo, Japan) for their help with data collection. This research was supported by a grant from the Korea Research Institute of Bioscience and Biotechnology Research Initiative Program.

REFERENCES

1. Tonks, N. K. (2006) Protein tyrosine phosphatases: from genes, to function, to disease. *Nat. Rev. Mol. Cell. Biol.* **7,** 833–846
2. Alonso, A., Sasin, J., Bottini, N., Friedberg, I., Friedberg, I., Osterman, A., Godzik, A., Hunter, T., Dixon, J., and Mustelin, T. (2004) Protein tyrosine phosphatases in the human genome. *Cell* **117,** 699–711
3. Rebay, I., Silver, S. J., and Tootle, T. L. (2005) New vision from Eyes absent: transcription factors as enzymes. *Trends Genet.* **21,** 163–171
4. Jemc, J., and Rebay, I. (2007) The eyes absent family of phosphotyrosine phosphatases: properties and roles in developmental regulation of transcription. *Annu. Rev. Biochem.* **76,** 24.1–24.26
5. Bonini, N. M., Leiserson, and, W. M., Benzer, S. (1993) The eyes absent gene: genetic control of cell survival and differentiation in the developing *Drosophila* eye. *Cell* **72,** 379–395
6. Pignoni, Hu, F., B., Zavitz, K. H., Xiao, J., Garrity, P. A., and Zipursky, S. L. (1997) The eye-specification protein So and Eya form a complex and regulate multiple step in *Drosophila* eye development. *Cell* **91,** 881–891
7. Chen, R., Amoui, M., Zhang, Z., and Mardon, G. (1997) Dachshund and eyes absent proteins form a complex and function synergistically to induce ectopic eye development in *Drosophila. Cell* **91,** 893–903
8. Rayapureddi, J. P., Kattamuri, C., Steinmetz, B. D., Frankfort, B. J., Ostrin, E. J., Mardon, G., and Hedge, R. S. (2003) Eyes absent represents a class of protein tyrosine phosphatases. *Nature* **426,** 295–298
9. Li, X., Oghi, K. A., Zhang, J., Krones, A., Bush, K. T., Glass, C. K., Nigam, S. K., Aggarwal, A. K., Maas, R., Rose, D. W., and Rosenfeld, M. G. (2003) Eya protein phosphatase activity regulates Six1-Dach-Eya transcriptional effects in mammalian organogenesis. *Nature* **426,** 247–254
10. Tootle, T. L., Silver, S. J., Davies, E. L., Newman, V., Latek, R. R., Mills, I. A., Selengut, J. D., Parlikar, B. E. W., and Rebay, I. (2003) The transcription factor Eyes absent is a protein tyrosine phosphatase. *Nature* **426,** 299–302
11. Epstein, J. A., and Neel, B. G. (2003) An eye on organ development. *Nature* **426,** 238–239
12. Cook, P. J., Ju, B., Telese, F., Wang, X., Glass, C. K., and Rosenfeld, M. G. (2009) Tyrosine dephosphorylation of H2AX modulates apoptosis and survival decisions. *Nature* **458,** 591–596
13. Krishnan, N., Jeong, D. G., Jung, S. K., Ryu, S. E., Xiao, A., Allis, C. D., Kim, S. J., and Tonks, N. K. (2009) Dephosphorylation of the C-terminal tyrosyl residue of the DNA damage-related histone H2A.X is mediated by the protein phosphatase eyes absent. *J. Biol. Chem.* **284,** 16066–16070
14. Burroughs, A. M., Allen, K. N., Dunaway-Mariano, D., and Aravind, L. (2006) Evolutionary genomics of the HAD superfamily. *J. Mol. Biol.* **361,** 1003–1034
15. Abdelhak, S., Kalatzis, V., Heilig, R., Compain, S., Samson, D., Vincent, C., Weil, D., Cruaud, C., Sahly, I., Leibovici, M., Bitnr-Glindzicz, M., Francis, M., Lacombe, D., Vigneron, J., Charachon, R., Boven, K., Bedbeder, P., Regemortr, N. V., Weissenbach, J., and Petit, C. (1997) A human homologue of the *Drosophila* eyes absent gene underlies branchio-oto-renal (BOR) syndrome and identifies a novel gene family. *Nat. Genet.* **15,** 157–164
16. Vincent, C., Kalatzis, V., Abdelhak, S., Chaib, H., Compai, S., Helias, J., Vaneecloo, F. M., and Petit, C. (1997) BOR and BO syndromes are allelic defects of EYA1. *Eur. J. Hum. Genet.* **5,** 242–246
17. Leslie, A. G. (1999) Integration of macromolecular diffraction data. *Acta Crystallogr. Allogr.* **D55**, 1696–1702
18. Collaborative Computational Project, Number 4, (1994) The CCP4 suite: programs for protein crystallography. *Acta Crystallogr. Allogr.* **D50,** 760–763
19. Otwinowski, Z., and Minor, W. (1997) Processing of X-ray diffraction data collected in oscillation mode. *Methods Enzymol.* **276,** 307–326
20. Terwilliger, T. C., and Berendzen, J. (1999) Automated MAD and MIR structure solution. *Acta Crystallogr. Allogr.* **D55,** 849–861

21. Jones, T. A., Zou, J. Y., Cowan, S. W., and Kjeldgaard, M. (1991) Improved methods for building protein models in electron density maps and the location of errors in these models. *Acta Crystallogr. Allogr.* **A47,** 110–119
22. Yeates, T. O. (1997) Detecting and overcoming crystal twinning. *Methods Enzymol.* **276**, 344–358
23. Brünger, A. T., Adams, P. D., Clore, G. M., DeLano, W. L., Gros, P., Grosse-Kunstleve, R. W., Jiang, J. S., Kuszewski, J., Nilges, M., Pannu, N. S., Read, R. J., Rice, L. M., Simonson, T., and Warren, G. L. (1998) Crystallography & NMR system: a new software suite for macromolecular structure determination. *Acta Crystallogr. Allogr.* **D54,** 905–921
24. Laskowski, R. A., MacArthur, M. W., Moss, D. S., and Thornton, J. M. (1993) PROCHECK: a program to check the stereochemical quality of protein structures. *J. Appl. Crystallogr.* **26,** 283–291
25. Carson, M. (1997) Ribbons. *Methods Enzymol.* **277,** 493–502
26. Kraulis, P. (1991) MOLSCRIPT: a program to produce both detailed and schematic plots of protein structures. *J. Appl. Crystallogr.* **24,** 946–950
27. Holm, L., and Sander, C. (1993) Protein structure comparison by alignment of distance matrices. *J. Mol. Biol.* **233,** 123–138
28. Wang, H., Pang, H., Bartlam, M., and Rao, Z. (2005) Crystal structure of human e1 enzyme and its complex with a substrate analog reveals the mechanism of its phosphatase/enolase. *J. Mol. Biol.* **348,** 917–926
29. Lu, Z., Dunaway-Mariano, D., and Allen, K. N., (2005) HAD superfamily phosphotransferase substrate diversification. *Biochemistry* **44,** 8684–8696
30. Ridder, I. S., Rozeboom, H. J., Kalk, K. H., and Dijkstra, B. W. (1999) Crystal structures of intermediates in the dehalogenation of haloalkanoates by L-2-haloacid dehalogenase. *J. Biol. Chem.* **274,** 30672–30678
31. Wang, W., Cho, H. S., Kim, R., Jancarik, J., Yokota, H., Nguyen, H. H., Grigoriev, I. V., Wemmer, D. E., and Kim, S. H. (2001) Crystal structure of phosphoserine phosphatase frm Methanococcus jannaschii, a hyperthermophile, at 1.8 Å resolution. *Structure* **9,** 65–72
32. Rayapureddi, J. P., Kattamuri, C., Chan, H. F., and Hegde, R. S., (2005) Characterization of a plant, tyrosine-specific phosphatase of the aspartyl class. *Biochemistry* **44,** 751–758
33. Zhang, Z. Y. (2002) Protein tyrosine phosphatases: structure and functions, substrate specificity, and inhibitor development. *Annu. Rev. Pharmacol. Toxicol.* **42,** 209–234
34. Wang, W., Cho, H. S., Kim, R., Jancarik, J., Yokota, H., Nguyen, H. H., Grigoriev, I. V., Wemmer, D. E., and Kim, S. H. (2002) Structural characterization of the reaction pathway in phosphoserine phosphatase: Crystallographic "snapshots" of intermediate states. *J. Mol. Biol.* **319,** 421–431
35. Ghosh, A., Shuman, S., and Lima, C. D. (2008) The structure of Fcp1, an Essential RNA polymerase II CTD phosphatase. *Mol. Cell.* **32,** 478–490
36. Mutsuddi, M., Chaffee, B., Cassidy, J., Silver, S. J., Tootle, T. L., and Rebay, I. (2005) Using *Drosophila* to decipher how mutations associated with human branchio-oto-renal syndrome and optical defects compromise the protein tyrosine phosphatase and transcriptional functions of eyes absent. *Genetics* **170,** 687–695
37. Ozaki, H., Watanabe, Y., Ikeda, K., and Kawakami, K. (2002) Impaired interactions between mouse Eya1 harboring mutations found in patients with branchio-oto-renal syndrome and Six, Dach, and G proteins. *J. Hum. Genet.* **47,** 107–116
38. Azuma, N., Hirakiyama, A., Inoue, T., Asaka, A., and Yamada, M. (2000) Mutations of a human homologue of the *Drosophila eyes absent* gene (*EYA1*) detected in patients with congenital cataracts and ocular anterior segment anomalies. *Hum. Mol. Genet.* **9,** 363–366
39. Migliosi, V., Flex, E., Guida, V., Martini, A., Markova, T., Torrente, I., and Dallapiccola, B. (2004) Identification of five novel BOR mutations in human EYA1 gene associated with branchio-oto-renal syndrome by a DHPLC-based assay. *Clin. Genet.* **66,** 478–480
40. Yin, S., Ding, F., and Dokholyan, N. V., (2007) Eris: an automated estimator of protein stability. *Nat. Methods* **4,** 466–467
41. Rayapureddi, J. P., and Hegde, R. S. (2006) Branchio-oto-renal syndrome associated mutations in eyes absent 1 result in loss of phosphatase activity. *FEBS Lett.* **580,** 3853–3859
42. Ikeda, K., Watanabe, Y., Ohto, H., and Kawakami, K., (2002) Molecular interaction and synergistic activation of a promoter by Six, Eya, and Dach proteins mediated through CREB binding protein. *Mol. Cell Biol.* **22,** 6759–6766
43. Bui, Q. T., Zimmerman, J. E., Liu, H., and Bonini, N. M. (2000) Molecular analysis of *Drosophila* eyes absent mutants reveals features of the conserved eya domain. *Genetics* **155,** 709–720

Received for publication August 10, 2009.
Accepted for publication September 24, 2009.